

This is a repository copy of *The role of humidity and UV-C emission in the inactivation of B. subtilis spores during atmospheric-pressure dielectric barrier discharge treatment.*

White Rose Research Online URL for this paper:

<https://eprints.whiterose.ac.uk/214457/>

Version: Published Version

Article:

Kogelheide, Friederike, Voigt, Farina, Hillebrand, Bastian et al. (6 more authors) (2020)
The role of humidity and UV-C emission in the inactivation of B. subtilis spores during atmospheric-pressure dielectric barrier discharge treatment. *Journal of Physics D: Applied Physics*. 295201. ISSN 0022-3727

<https://doi.org/10.1088/1361-6463/ab77cc>

Reuse

This article is distributed under the terms of the Creative Commons Attribution (CC BY) licence. This licence allows you to distribute, remix, tweak, and build upon the work, even commercially, as long as you credit the authors for the original work. More information and the full terms of the licence here:

<https://creativecommons.org/licenses/>

Takedown

If you consider content in White Rose Research Online to be in breach of UK law, please notify us by emailing eprints@whiterose.ac.uk including the URL of the record and the reason for the withdrawal request.

PAPER • OPEN ACCESS

The role of humidity and UV-C emission in the inactivation of *B. subtilis* spores during atmospheric-pressure dielectric barrier discharge treatment

To cite this article: Friederike Kogelheide *et al* 2020 *J. Phys. D: Appl. Phys.* **53** 295201

View the [article online](#) for updates and enhancements.

You may also like

- [Sporicidal properties from surface micro-discharge plasma under different plasma conditions at different humidities](#)
J Jeon, T G Klaempfl, J L Zimmermann et al.
- [Sterilization/disinfection using reduced-pressure plasmas: some differences between direct exposure of bacterial spores to a discharge and their exposure to a flowing afterglow](#)
M Moisan, P Levif, J Séguin et al.
- [Influence of spore size distribution, gas mixture, and process time on the removal rate of *B. subtilis* spores in low-pressure plasmas](#)
Marcel Fiebrandt, Julian Roggendorf, Ralf Moeller et al.

PRIME
PACIFIC RIM MEETING
ON ELECTROCHEMICAL
AND SOLID STATE SCIENCE

HONOLULU, HI
October 6-11, 2024

Joint International Meeting of
The Electrochemical Society of Japan
(ECS)
The Korean Electrochemical Society
(KECS)
The Electrochemical Society (ECS)

Early Registration Deadline:
September 3, 2024

**MAKE YOUR PLANS
NOW!**

The role of humidity and UV-C emission in the inactivation of *B. subtilis* spores during atmospheric-pressure dielectric barrier discharge treatment

Friederike Kogelheide¹ , Farina Voigt¹, Bastian Hillebrand¹, Ralf Moeller², Felix Fuchs¹ , Andrew R. Gibson^{1,3} , Peter Awakowicz¹, Katharina Stapelmann⁴  and Marcel Fiebrandt¹ 

¹ Institute of Electrical Engineering and Plasma Technology, Faculty of Electrical Engineering and Information Sciences, Ruhr University Bochum, Bochum, Germany

² Department of Radiation Biology, Space Microbiology Research Group, German Aerospace Center (DLR e.V.), Institute of Aerospace Medicine, Cologne, Germany

³ Research Group for Biomedical Plasma Technology, Faculty of Electrical Engineering and Information Sciences, Ruhr University Bochum, Bochum, Germany

⁴ Department of Nuclear Engineering, North Carolina State University, Raleigh, NC 27695, United States of America

E-mail: kogelheide@aept.rub.de and fiebrandt@aept.rub.de

Received 5 December 2019, revised 10 January 2020

Accepted for publication 18 February 2020

Published 19 May 2020



CrossMark

Abstract

Experiments are performed to assess the inactivation of *Bacillus subtilis* spores using a non-thermal atmospheric-pressure dielectric barrier discharge. The plasma source used in this study is mounted inside a vacuum vessel and operated in controlled gas mixtures. In this context, spore inactivation is measured under varying nitrogen/oxygen and humidity content and compared to spore inactivation using ambient air. Operating the dielectric barrier discharge in a sealed vessel offers the ability to distinguish between possible spore inactivation mechanisms since different process gas mixtures lead to the formation of distinct reactive species. The UV irradiance and the ozone density within the plasma volume are determined applying spectroscopic diagnostics with neither found to fully correlate with spore inactivation. It is found that spore inactivation is most strongly correlated with the humidity content in the feed gas, implying that reactive species formed, either directly or indirectly, from water molecules are strong mediators of spore inactivation.

Keywords: dielectric barrier discharge, inactivation experiments, spectroscopy, atmospheric pressure, controlled atmosphere, *Bacillus subtilis* spores

(Some figures may appear in colour only in the online journal)

1. Introduction

A variety of physical and chemical means, such as heat, chemical vapor or radiation, offer the possibility to achieve the

inactivation of harmful microorganisms. However, the accompanying material damage of most conventional sterilisation methods cannot be neglected [1]. In particular, any application designed to reduce bacterial load on living tissue must demonstrate minimal risk for patients while showing clinical effectiveness in the inactivation of harmful microorganisms. Due to their low gas temperatures, non-thermal plasmas produced at atmospheric pressure are a promising approach for such



Original Content from this work may be used under the terms of the [Creative Commons Attribution 4.0 licence](https://creativecommons.org/licenses/by/4.0/). Any further distribution of this work must maintain attribution to the author(s) and the title of the work, journal citation and DOI.

applications. These plasmas produced in air and other gas mixtures have been demonstrated to cause inactivation of microorganisms on treated surfaces and in human wounds [2–8]. Significant effort has been made in recent years to understand the mechanisms of deactivation. For example, the work of Krewing *et al* used *E. coli* mutants to identify 87 genes that confer a certain level of resistance against treatment using the effluent of a He/O₂ plasma jet [9]. By exposing these mutants to individual stressors expected to be present during plasma exposure, the authors were able to conclude that most genes acted to protect bacteria from hydrogen peroxide, superoxide and/or nitric oxide. These results provide a strong indication that these species are important mediators of plasma induced effects under the conditions studied by the authors. In addition, using a combination of UV radiation measurements, under different plasma conditions and inactivation experiments, Reineke *et al* were able to demonstrate that UV radiation played an important role in the inactivation of *B. subtilis* spores exposed to an Ar/O₂/N₂ plasma jet [10]. Moreover, Klämpfl *et al* showed that different spores can also be inactivated using an atmospheric surface microdischarge plasma source in a closed environment, suggesting that the inactivation might be related to ozone [11]. However, despite a large number of studies demonstrating the inactivation of microorganisms as a result of plasma treatment, a complete picture of which plasma-produced components are important under a particular operating condition is still to be formed. This is in large part due to the wide range of reactive components delivered by non-thermal plasmas and the difficulty in measuring all relevant components for a given treatment condition. This issue is compounded by the wide variety of plasma sources used for such studies that each deliver different quantities of reactive components.

With respect to the effects on living tissues, it has been shown that plasma-produced molecules, such as nitric oxide, are capable of promoting wound healing [12, 13]. Contact-free and painless application of these plasmas to human tissue has also been demonstrated in clinical studies [14]. The possibility to induce favourable effects in tissues while also exerting antimicrobial activity means that non-thermal plasmas have a wide variety of potential applications in biomedicine. However, the widespread and effective use of these devices in biomedical applications requires further knowledge of their mechanisms of interactions with biological systems so that the plasma properties can be optimised for applications. This view is supported by the recent meta-analysis of clinical studies of non-thermal plasmas for chronic wound healing by Assadian *et al* [15]. This analysis concluded that the use of non-thermal plasmas for chronic wound healing has been demonstrated to be safe, however, no statistically significant clinical benefit in terms of reduction in wound size or bioburden has yet been demonstrated compared to standard chronic wound treatments. To overcome this challenge, additional fundamental research on the mode of action of plasma sources in medical applications is needed to point towards favourable plasma regimes to maximise beneficial effects, such as a reduction in bacterial load.

The Gram-positive spore-forming bacterium *Bacillus subtilis* is one of the most extensively characterised microorganisms. Several bacteria are able to form endospores to protect their DNA in case of severe outer stressors, such as UV emission, heat, lack of nutrition or chemicals. *Bacillus subtilis* is able to form dormant endospores under extreme environmental stress, such as nutrient and water deprivation. In their spore form, bacteria do not show metabolism, but do show significantly increased resistance to stressors compared to their vegetative form. Briefly, this is achieved by discarding irrelevant components from the vegetative cell and forming several protective layers called the spore coat. In addition, DNA is further protected by small acid-soluble proteins (SASP), in a spore-specific calcium dipicolinic acid (Ca-DPA) environment at the core. The core and spore coat are separated by the cortex which exhibits two membranes to enable nutrition transport into the spore, if the surroundings are favourable again. Dormant spores harbor the most efficient protection mechanisms among bacteria and have therefore served in several studies as a model to verify sterilization and inactivation methods, biodosimetry, and are also used as the gold standard to regularly evaluate and test standard sterilization procedures [16]. Furthermore, the non-pathogenic nature of *B. subtilis* makes it an ideal model organism for many scientific and industrial purposes [16–18]. Detailed information on the spore structure and protection mechanisms can be found in [19–21].

In this work, the inactivation of *B. subtilis* spores by a dielectric barrier discharge (DBD) is studied. To distinguish and evaluate the impact of possible mechanisms by which atmospheric-pressure plasmas lead to the inactivation of bacterial spores the composition of the process gas was changed in a controlled manner. The influence of the gas composition on the absolute UV irradiance and ozone (O₃) concentration, two prominent biologically active components of the plasma, was determined using emission and absorption spectroscopy, respectively. This approach offers the ability to determine whether or not these components play a prominent role in spore inactivation.

The manuscript is structured in the following way: in section 2, the experimental setup, as well as the handling protocol of the spores, is described in detail. Additionally, the experimental setups used for optical emission and absorption spectroscopy are introduced and the geometrical factor needed to determine the absolute UV irradiance on any treated biological sample is established. In section 3, the results of the inactivation experiments as well as the absolute UV irradiance and ozone concentrations are described. Finally, the results are discussed in section 4, with a focus on potential inactivation mechanisms.

2. Experimental procedures

2.1. Experimental setup

The DBD used in this work consists of a cylindrical copper electrode covered by aluminium oxide (Al₂O₃) and driven by a self-built pulsed power supply [22]. The driven electrode has

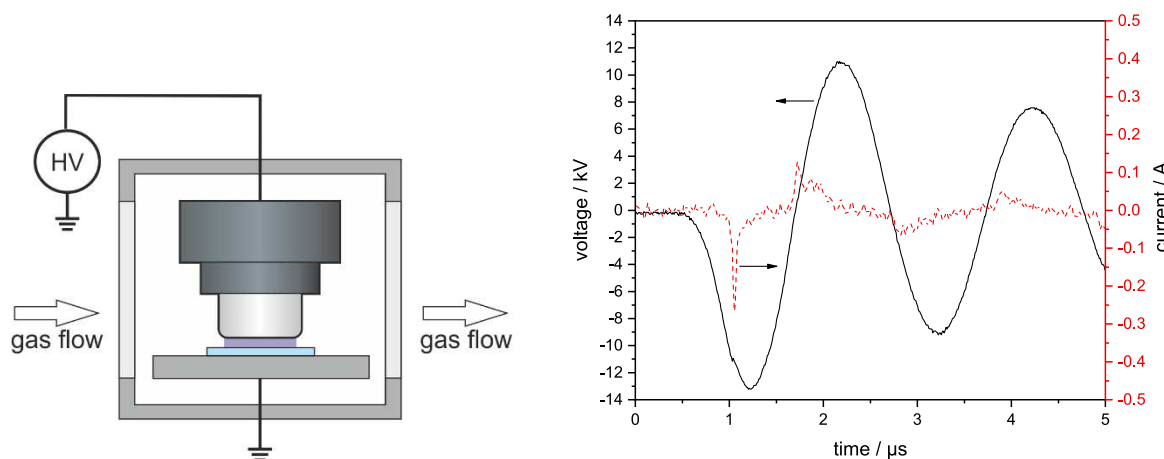


Figure 1. Sketch of the experimental setup of the DBD inside a vessel (left) and the corresponding voltage and conduction current characteristics of the DBD for a pulse repetition frequency of $f = 1000$ Hz and a peak-to-peak voltage of 24 kV_{pp} (right). [22] John Wiley & Sons. © 2019 WILEY-VCH Verlag GmbH & Co. KGaA, Weinheim.

a diameter of 10 mm, including the dielectric, and the distance between the dielectric and the treated sample is kept constant at 1 mm for all experiments. In figure 1, a sketch of the experimental setup of the DBD is presented. The DBD is driven by damped sine wave pulses with a frequency of around 500 kHz as depicted in figure 1 (right). The pulse repetition frequency can be varied between 100 Hz and 4 kHz and the high voltage amplitude can be set within the range of 0 kV_{pp} to 28 kV_{pp} . For the determination of the power deposited in the plasma, an electrical characterisation of the discharge is carried out. This is done according to Kogelheide *et al* [22]. Voltage and current measurements are conducted using a capacitive voltage divider (P6015A, Tektronix, USA), a current monitor (Model 2877, Pearson Electronics, USA) and a digital oscilloscope (LeCroy9459 DUAL 350 MHz, LeCroy, USA). In figure 1 (right), the current-voltage characteristics of the discharge are displayed after subtraction of the displacement current [22]. The DBD is placed inside a vacuum vessel made of aluminium which is mounted to a miniature flow passage and a vacuum pump (Trivac D16BCS-PFPE, Leybold, Germany) in order to operate the DBD in a defined atmosphere. The total gas flow is adjusted via two mass flow controllers (El-Flow Prestige, Bronkhorst, Germany) and amounts to 2 slm. In this study, different nitrogen/oxygen (purity 5.0, Air Liquide, Germany) gas mixtures, namely $\text{N}_2:\text{O}_2$ 99.9%:0.1%, 80%:20%, 50%:50%, 20%:80% and 0.1%:99.9%, are chosen as the process gas. For experiments carried out in synthetic air ($\text{N}_2:\text{O}_2$ 79%:21%) in combination with different humidity content, the feed gas is partly passed through a gas washing bottle filled with distilled water. The relative humidity as a function of the fraction of the feed gas passed through the gas washing bottle is measured inside the vacuum vessel prior to the experiments using a humidity probe (Testo 435, Testo SE & Co KGaA, Germany). The pressure inside the vessel is set to 1 bar using an adjustable valve and a vacuum pump. To control and monitor the pressure inside the vessel, a pressure gauge (Baratron 750-C, MKS, USA) and pressure controller (Model 250, MKS, USA) are used. All inactivation measurements are carried out by placing the spore covered sample on a grounded aluminium

plate underneath the driven electrode inside the vacuum vessel.

2.2. Bacterial strains, sporulation and spore purification

Spores of *B. subtilis* (strain PY79, a prototrophic laboratory strain with wild-type DNA repair and spore protection capabilities) are obtained by the cultivation of vegetative cells under vigorous aeration at 37°C for 7 days in double-strength liquid Schaeffer sporulation medium [23]. Afterwards, the spores are purified and stored as described in [24,25]. The prepared spores consisted of a suspension of single spores with no detectable clumps, and were free (>99%) of growing cells, germinated spores, and cell debris, as verified using a phase-contrast microscope [26].

2.3. Preparation of spore samples

To ensure a homogeneous and reproducible treatment of the samples, the spores are deposited on glass substrates with a diameter of 11 mm by spray deposition. The glass slides used were chosen to be larger in diameter than the driven electrode of the DBD to ensure that the discharge does not interact with the rough edges of the glass substrates making the plasma less homogeneous. The disadvantages of this arrangement, such as the decaying photon flux and radical densities towards the edges, are discussed in section 4. A self-built spray device described in [27], based on a similar device presented in [28], is used. A spore solution of 5×10^9 spores ml^{-1} is sprayed for 150 ms using 1.3 bar nitrogen (purity 5.0, Air Liquide, Germany) as the carrier gas. To verify the homogeneity of the sprayed solution and to check if the spores are present in a monolayer on the substrate, scanning electron microscopy (JSM6510, JEOL, Eching, Germany) is performed.

2.4. Treatment conditions

The samples are placed on a sample holder made specifically for the glass slides used to ensure that every sample is placed directly underneath the electrode in a reproducible way.

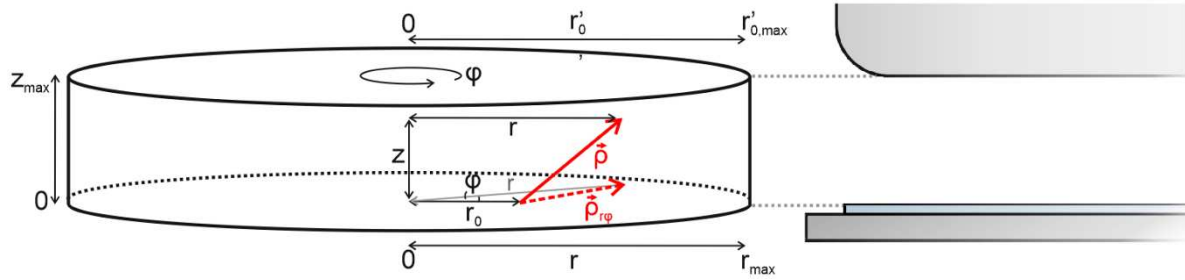


Figure 2. Sketch of the plasma volume for the calculation of the geometrical factor to determine the density of irradiance generated in the plasma volume that reaches the sample surface.

All samples are handled in the same way: first, the sample is placed inside the vessel on the sample holder. Then, the vessel is evacuated down to approximately 1 mbar in order to minimise the impact of impurities during the plasma treatment. In order to ensure stable conditions during the plasma treatment, the composition of the process gas, as well as the pressure, is adjusted thereafter. Finally, the sample is treated with the DBD.

In this study, the samples are treated with DBD produced in different mixtures of nitrogen/oxygen/humidity and power densities. Unless stated otherwise, all experiments were carried out with a pulse repetition frequency of 300 Hz and a maximum voltage amplitude of 24 kV_{pp}.

2.5. Spore survival assay

After the plasma treatment, each sample is covered with 60 μl of 10% polyvinyl alcohol (PVA) solution to remove more than 95% of the spores from the glass slides [29]. The PVA is applied to an area with a radius of 10 mm to exclude spores at the edge of the sample carriers for two reasons: firstly, the edges of the sample carriers show small fractures from the manufacturing process. Spores lying in cavities or trenches would be likely to be shielded from UV emission and radicals which would influence the reproducibility of the samples. Secondly, as shown in the results section, the flux of reactive plasma components changes significantly from the center of the electrode to the side. To reduce the influence of this effect only spores located in the plasma region are taken into account for the analysis. The PVA coated samples were dried on a clean bench until the PVA layer was completely solidified. The dried PVA film is then removed from the substrate and dissolved in 120 μl water. This procedure makes it possible to recover spores without affecting their viability [18]. Afterwards, serial dilutions of the recovered samples are plated on LB agar plates as described previously in [27]. Plates are then incubated overnight at 37 °C, after which, colonies are counted. Plates with a number of colonies between 1 and 1000 are included in the calculation of the survival rates. For higher numbers, overlapping or merging of the colonies is observed. All data shown are expressed as averages (±) standard deviations (n = 3, 10).

2.6. Optical emission spectroscopy

For the determination of the UV irradiance experienced by the biological samples, absolute measurements were performed using an echelle spectrometer (ESA 4000, LLA Instruments, Germany). The spectrometer has a spectral range between 200 nm and 800 nm with a spectral resolution of 0.015 nm < Δλ < 0.06 nm. To calculate the UV irradiance absolutely calibrated intensities have to be obtained. The calibration procedure as well as the determination of absolute intensities is described in detail in [30]. As a result, the number of photons s⁻¹ nm⁻¹ at the fibre entrance I_{abs}(λ) is known. To calculate the UV irradiance experienced by the biological samples, an aperture is used to define the plasma volume (V_{plasma}) seen by the optical fibre. Therewith, the average emissivity of the plasma ε(λ) in photons s⁻¹ nm⁻¹ cm⁻³ can be determined. This procedure assumes a homogeneous plasma emission in the whole volume which was demonstrated for N₂ emission using a CCD camera in [31]. However, as the sample carrier in contact with the discharge has the same dimension as the electrode and the plasma volume, the irradiance experienced by the spores strongly depends on their position on the sample carrier. This is the case as each emitting particle in the plasma volume radiates homogeneously in 4π and the fraction of light reaching the sample depends on the distance between the emitting particle and the sample. Figure 2 shows a sketch of the plasma volume with the electrode at the top and the sample at the bottom of the plasma cylinder. The particles in the volume r dφ dr dz irradiate their emission on a surface of a sphere of 4πρ² with ρ = √(r² + z²) being the sphere radius. If the radiation reaches the surface tilted, the effective area of the surface seen by the particle decreases and has to be corrected with the cosine of the angle between surface normal and photon yielding cos(arctan(r/z)) = √((z/r)² + 1)⁻¹. Thus, the geometrical factor to calculate the irradiance at the center of the sample carrier G₀ generated by the whole plasma volume is given by

$$G_0 = \int_0^{z_{\max}} \int_0^{r_{\max}} \int_0^{2\pi} \frac{1}{4\pi\rho^2} \frac{1}{\sqrt{\left(\frac{r}{z}\right)^2 + 1}} r d\varphi dr dz. \quad (1)$$

To determine the photon flux on the sample at positions off the center, the position on the sample carrier has to be shifted by r₀. Due to the rotational symmetry the resulting value is

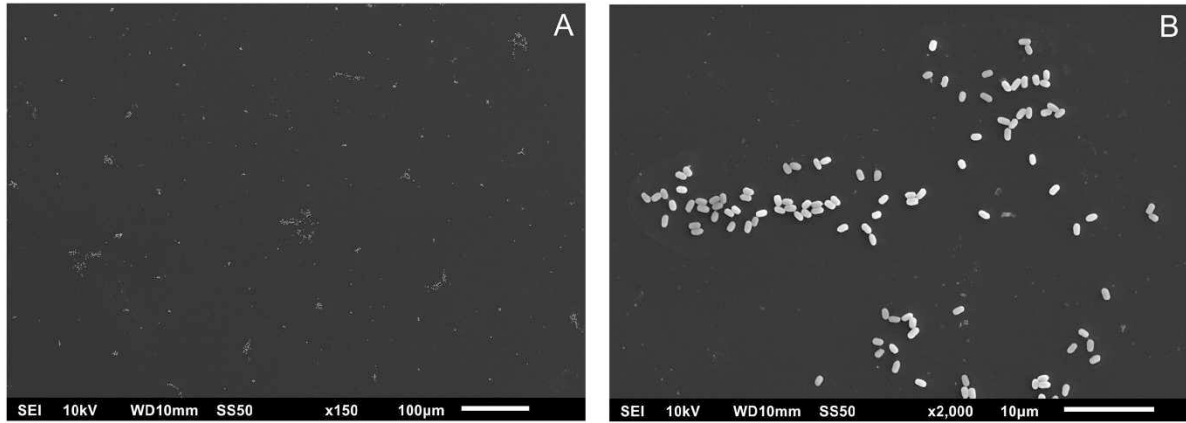


Figure 3. SEM images of the sprayed *B. subtilis* spores on glass slides in the center of the sample carrier with magnification of 150 (A) and 2000 (B). No stacked spores are observed.

valid on a circle with radius r_0 . By shifting the point of irradiance, the distance ρ to the emitting particle changes. As the distance in z-direction is not affected by the change of ρ , ρ only depends on the shift in the $r - \varphi$ - plane. Figure 2 depicts the resulting projection of ρ on the sample plane $\rho_{r\varphi}$. As r , r_0 , and φ are known, $\rho_{r\varphi}$ can be determined using the cosine rule:

$$\rho_{r\varphi}^2 = (r - r_0 \cos(\varphi))^2 + (r_0 \sin(\varphi))^2 \quad (2)$$

Therefore, the geometrical factor to calculate the irradiance at distance r_0 to the center $G(r_0)$ is

$$G(r_0) = \int_0^{z_{\max}} \int_0^{r_{\max}} \int_0^{2\pi} \frac{1}{4\pi(\rho_{r\varphi}^2 + z^2)} \frac{1}{\sqrt{\left(\frac{\rho_{r\varphi}}{z}\right)^2 + 1}} r d\varphi dr dz. \quad (3)$$

Due to the symmetry of the system, $G(r_0)$ is also valid for the upper electrode with the aluminium oxide cover which has a reflectivity of around 90% in the UV range [32, 33]. Thus, to determine the total irradiance reaching the sample, the reflection from the electrode must also be taken into account. For this, a diffuse reflection of the irradiance $G(r'_0)$ at any point (r'_0, z_{\max}) on the aluminum oxide is assumed (note that the upper radial vector is chosen to r'_0 and the radial vector on the sample carrier to r_0). Each point is a radiating surface emitting into a half sphere. The half sphere radius is the distance between the reflection point r'_0, z_{\max} to the point on the sample $(r_0, 0)$. As in the first case, the z-component is constant and the change in the radius is determined by the projection of the distance vector on the $r - \varphi$ - plane $\rho'_{r\varphi}$ which is again calculated with the cosine rule:

$$\rho'_{r\varphi}{}^2 = (r'_0 - r_0 \cos(\varphi))^2 + (r_0 \sin(\varphi))^2. \quad (4)$$

In addition, the effective area of the reflecting upper electrode and of the sample carrier have to be taken into account using a cosine correction as the line-of-sight from the emission point (r'_0, z_{\max}) to the observation point $(r_0, 0)$ is not parallel to the

normal of both surfaces. Thus, the geometrical factor to calculate the reflected irradiance from the upper electrode to a point on the sample carrier $G_{\text{refl}}(r_0)$ is determined with

$$G_{\text{refl}}(r_0) = 0.9 \cdot \int_0^{r'_{0,\max}} \int_0^{2\pi} G(r'_0) \frac{1}{2\pi(\rho'_{r\varphi}{}^2 + z_{\max}^2)} \frac{1}{\left(\frac{\rho'_{r\varphi}}{z_{\max}}\right)^2 + 1} r'_0 dr'_0 d\varphi'. \quad (5)$$

Therewith, the total geometrical factor to determine the irradiance at a point on the sample carrier $G_{\text{tot}}(r_0)$ assuming a homogeneous discharge with constant emissivity and a reflectivity of the upper electrode of 90% is

$$G_{\text{tot}}(r_0) = G(r_0) + G_{\text{refl}}(r_0). \quad (7)$$

By taking the constant emissivity $\varepsilon(\lambda)$ and the photon energy $\frac{hc}{\lambda}$ of a photon with wavelength λ , the Planck constant h and the speed of light c into account, the UV energy flux at a position r_0 on the sample carrier $[UV](r_0)$ in $\text{Joule s}^{-1} \text{cm}^{-2}$ or the total UV energy flux on the sample carrier $[UV]$ in Joule s^{-1} is calculated:

$$[UV](r_0) = \int_{UV} \varepsilon(\lambda) \frac{hc}{\lambda} G_{\text{tot}}(r_0) d\lambda \quad (8)$$

$$[UV] = 2\pi \int_0^{r_{0,\max}} [UV](r_0) r_0 dr_0. \quad (9)$$

2.7. Optical absorption spectroscopy

Absolute densities of ozone are determined by applying absorption spectroscopy within the range of $\lambda = 200\text{--}320$ nm. A deuterium lamp (L9518, Hamamatsu Photonics K.K, Japan) and a broad-band spectrometer (QE65000, Ocean Optics, Germany) are used, as well as two parabolic mirrors (effective focal length = 25 cm), in order to establish a collimated light

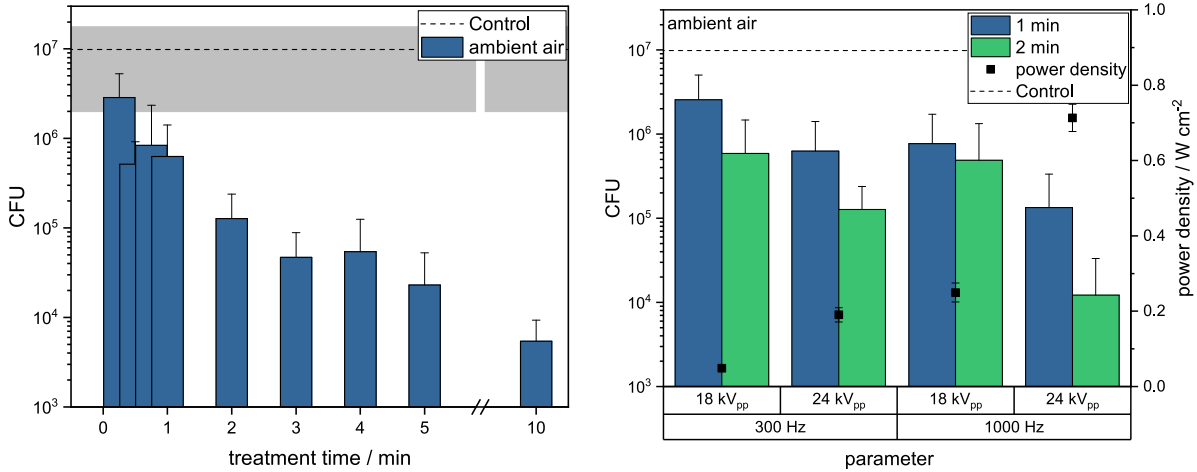


Figure 4. Spore inactivation by atmospheric-pressure DBD formed in ambient air: Colony forming units of wild-type *B. subtilis* spores treated with plasma for various times at 300 Hz and 24 kV_{pp} (left) and varying power density after 1 min and 2 min (right). The dashed line represents the untreated sample. The data is expressed as averages (n = 10) and the standard deviation is displayed as error bars. The error bar of the control measurement is represented by the grey area (left).

beam. The light emitted from the deuterium lamp is collimated by a mirror into a parallel beam which is directed through the plasma volume onto another mirror. This second mirror is used to focus the light beam onto the entrance of the optical fibre connected to the spectrometer. The absolute densities of ozone are determined applying the Beer–Lambert law.

$$I_T(\lambda) = I_0(\lambda) \cdot \exp(-\sigma_{253\text{nm}}(\lambda) \cdot n_{\text{O}_3} \cdot l). \quad (10)$$

In equation (10), $I_T(\lambda)$ denotes a measured signal that is transmitted through the medium, $I_0(\lambda)$ denotes the second measured signal without absorption but along an identical path, $\sigma(\lambda)$ and n_{O_3} denote the absorption cross section and the density of the absorbing medium, and l denotes the length of the absorption path. Dividing by $I_0(\lambda)$, applying the natural logarithm, and rearranging for n_{O_3} yields the density. To correct the incident and the transmitted spectral intensity $I_0(\lambda)$ and $I_T(\lambda)$ for the background signal as well as the plasma emission, four measurements are needed:

$$\frac{I_T(\lambda)}{I_0(\lambda)} = \frac{I_{\text{plasma on, lamp on}}(\lambda) - I_{\text{plasma on, lamp off}}(\lambda)}{I_{\text{plasma off, lamp on}}(\lambda) - I_{\text{plasma off, lamp off}}(\lambda)}. \quad (11)$$

$I_{\text{plasma on, lamp on}}(\lambda)$ represents the intensity of the light source with the plasma source ignited and $I_{\text{plasma on, lamp off}}(\lambda)$ the plasma emission which has to be taken into account. The intensity of the light source $I_{\text{plasma off, lamp on}}(\lambda)$ is corrected for the background signal $I_{\text{plasma off, lamp off}}(\lambda)$. The absorption cross section of ozone $\sigma_{253\text{nm}}$ at $\lambda = 253.65$ nm, the maximum of the Hartley absorption band [34], is used. The head of the Hartley absorption band is used because this part of the band mainly represents the absorption due to ozone molecules in the ground state while the edges of the band are slightly more sensitive to vibrationally excited ozone molecules which are sensitive to the gas temperature [35]. The temperature dependence is accounted for via a polynomial fit derived from the data presented in [35].

3. Results

3.1. Spore sample preparation

The stacking of spores can significantly influence the results of inactivation experiments due to the shadowing, and thus, protection of lower lying spores by spores on top [28]. The spore distribution was checked as described in section 2.3. Figure 3 shows examples of the spore distribution on the glass slides at different magnification values. No stacking of spores is observed; hence, the influence on the inactivation results due to the shadowing effect should be minimised.

3.2. Inactivation of spores in ambient air

The number of colony forming units (CFU) measured after the treatment of *B. subtilis* spores in ambient air, without humidity control (typical humidity of ambient air is 45%–55% in this case), are shown as a function of treatment time in figure 4 (left). The spores were treated for various times from 10 s up to 10 min. The dashed, black line represents the untreated control. In the first three minutes, the CFU count is reduced by two orders of magnitude following an approximately exponential trend. Afterwards, the inactivation efficiency decreases resulting in an additional reduction of only one log in the next seven minutes.

The influence of the power density on the CFU count is depicted in figure 4 (right). The power density is controlled by changing the repetition frequency between 300 Hz and 1000 Hz and the voltage amplitude between 18 kV_{pp} and 24 kV_{pp}. The fraction of surviving spores were determined after 1 min and 2 min treatment time. In general, the reduction of CFU correlates with the power density with CFU count after 2 minute treatments decreasing by approximately 1.5 log from the lowest to the highest power density.

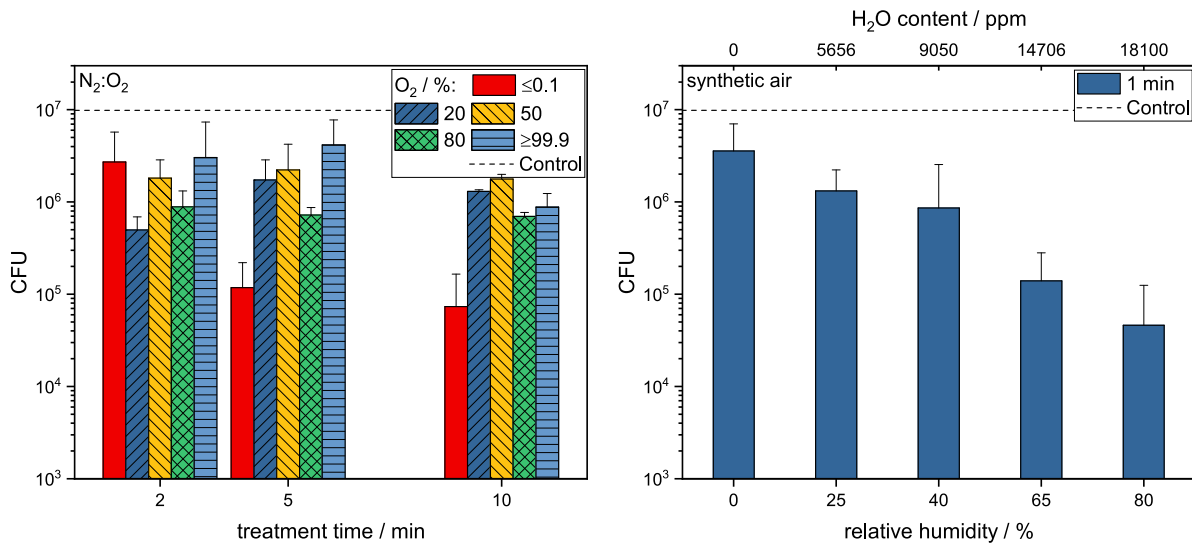


Figure 5. Results of the inactivation experiments of *B. subtilis* spores treated with the DBD operated in different dry nitrogen/oxygen gas mixtures for 2 min, 5 min and 10 min (left) and in synthetic air with controlled relative humidity for 1 min (right). The experiments were carried out using the DBD set to 300 Hz and 24 kV_{pp}. The dashed line represents the untreated sample. The data is expressed as averages (n = 3) and the standard deviation is displayed as error bars.

3.3. Inactivation of spores in humidity controlled nitrogen/oxygen atmospheres

The following results were obtained using a sealed vessel to control the atmospheric conditions under which the inactivation experiments were performed. Figure 5 (left) depicts CFU counts after *B. subtilis* spore treatment in dry atmosphere with varying nitrogen/oxygen content. In general, the results of treatments using gas mixtures with an oxygen content ≥20% are comparable, resulting in a small reduction in CFU count of approximately one log after 10 min. Interestingly, in a nitrogen atmosphere with oxygen residuals (≤0.1%) the CFU count decreases more quickly showing a two log decrease in the same treatment time. However, this reduction is already achieved after 5 min suggesting that prolonged treatment times have only a minor effect. An oxygen fraction of ~0.1% corresponds to the impurities in the vacuum vessel during the inactivation experiments using pure nitrogen as process gas. This impurity content was estimated applying optical emission spectroscopy by comparing the spectrum of the DBD obtained during the inactivation experiments, with only nitrogen gas fed into the chamber, to spectra of the DBD ignited in nitrogen with distinct admixtures of oxygen. While this approach does not allow for the measurement of a precise impurity content, it does allow for the order of magnitude of the oxygen impurities to be assessed.

The influence of the relative humidity content on the inactivation efficiency of *B. subtilis* spores in synthetic air (N₂:O₂ 79%:21%) is depicted in figure 5 (right). Treatment times of 1 min are compared for 0%, 25%, 40%, 65%, and 80% relative humidity. The addition of water vapour strongly increases the inactivation efficiency from less than one order of magnitude in dry air up to approximately two orders of magnitude at 80% relative humidity. The rise in efficiency scales nearly exponentially with the relative humidity increase.

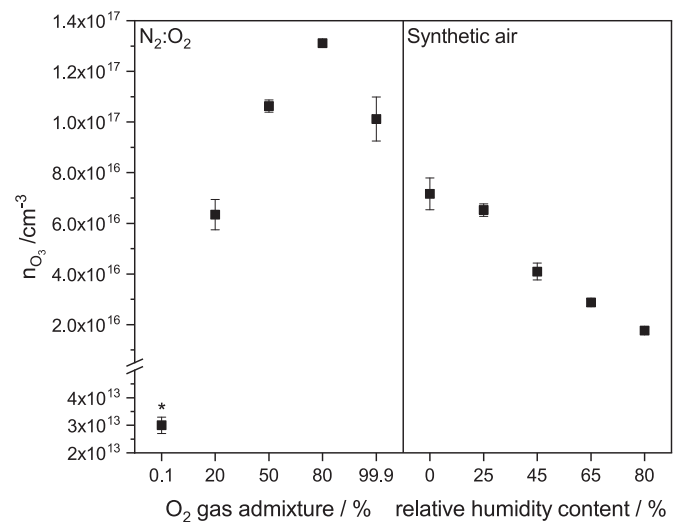


Figure 6. Ozone density measured in the plasma volume of the DBD operated in different nitrogen/oxygen mixtures (left) and in synthetic air with varying relative humidity (right) (f = 300 Hz, V_{pp} = 24 kV_{pp}). The data is expressed as averages (n = 3) and the standard deviation is displayed as error bars. * indicates the detection limit of ozone based on the method used.

3.4. Ozone density in humidity controlled nitrogen/oxygen atmosphere

Figure 6 depicts the volume averaged ozone density produced by the DBD in dry nitrogen/oxygen mixtures and with varying relative humidity in synthetic air. In a dry atmosphere, the ozone density is highest at an oxygen content of 80% reaching a value of 1.3 × 10¹⁷ cm⁻³. In nearly pure oxygen and with 50% nitrogen the density of ozone is similar at 1.1 × 10¹⁷ cm⁻³. With increasing nitrogen content the ozone density

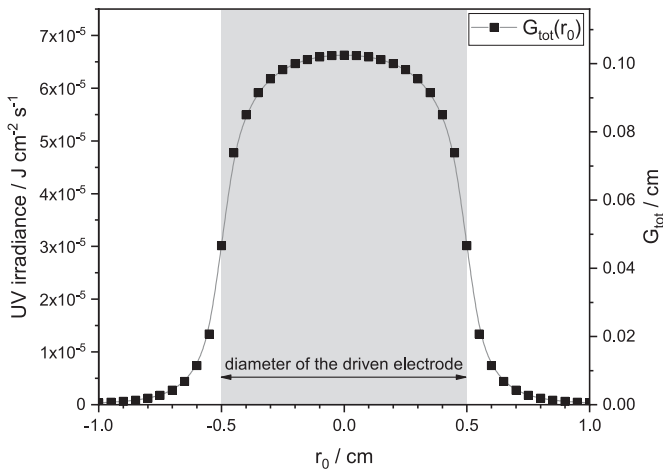


Figure 7. The radial profile of the UV irradiance in a N₂:O₂ mixture of 80%:20% (proportional to the geometric factor G_{tot} , shown on the right hand axis) as a function of radius r_0 (equation (7)). The grey area indicates the diameter of the driven electrode and the region of homogeneous photon emission.

strongly decreases to $6.2 \times 10^{16} \text{ cm}^{-3}$ at 80% nitrogen content and below the detection limit ($n_{O_3} = 3.0 \times 10^{13} \text{ cm}^{-3}$) in nearly pure nitrogen atmosphere. In synthetic air (N₂:O₂ 79%:21%) the addition of water into the gas phase significantly reduces the ozone concentration in the discharge. In a dry atmosphere the ozone density is $7.0 \times 10^{16} \text{ cm}^{-3}$ and decreases to nearly a third at 80% relative humidity.

3.5. UV dose in humidity controlled nitrogen/oxygen atmosphere

The diameter of the Al₂O₃-covered, driven electrode and the sample carrier are nearly identical which results in an inhomogeneous irradiation of the spores even in the case of a homogeneous discharge below the whole electrode. The irradiance profile, determined with equation (7), as a function of radial distance from the center of the sample carrier is shown in figure 7 as well as the exemplary UV irradiance profile in a N₂:O₂ mixture of 80%:20% calculated with equation (9). The calculations show that spores in a circle of 0.4 cm radius in the center of the discharge experience a similar irradiance. However, with increasing distance the photon flux is significantly reduced, down to 50% at the edge of the driven electrode at $r_0 = 0.5 \text{ cm}$ and to 10% at $r_0 = 0.6 \text{ cm}$ (outside of the active plasma zone). Thus, the UV irradiance changes significantly depending on the position of the spore on the sample carrier and has to be taken into account in the interpretation of the inactivation results. To compare the UV irradiance for different gas mixtures, the photon flux, separated into different wavelength ranges, at the center of the sample carrier is given in figure 8 for each treatment condition. Only in nitrogen with residual oxygen a significant amount of UV-C emission is produced resulting from the formation of NO and emission from the NO_γ band (NO(A-X)) [36]. This can be observed in the emission spectra shown in figure 9, for the DBD operated in a N₂:O₂ mixture of 99.9%:≤0.1% and

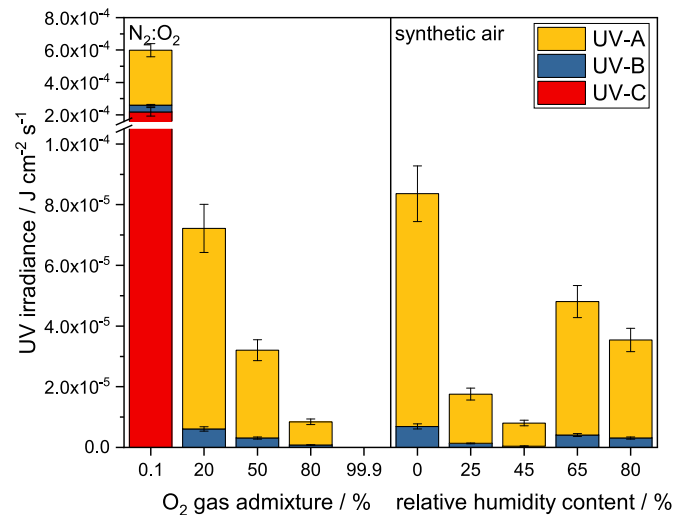


Figure 8. UV irradiance at the centre of the sample carrier for the DBD operated in different nitrogen/oxygen mixtures (left) and in synthetic air with varying humidity content ($f = 300 \text{ Hz}$, $V_{pp} = 24 \text{ kV}_{pp}$). The data is expressed as averages ($n = 3$) and the standard deviation is displayed as error bars.

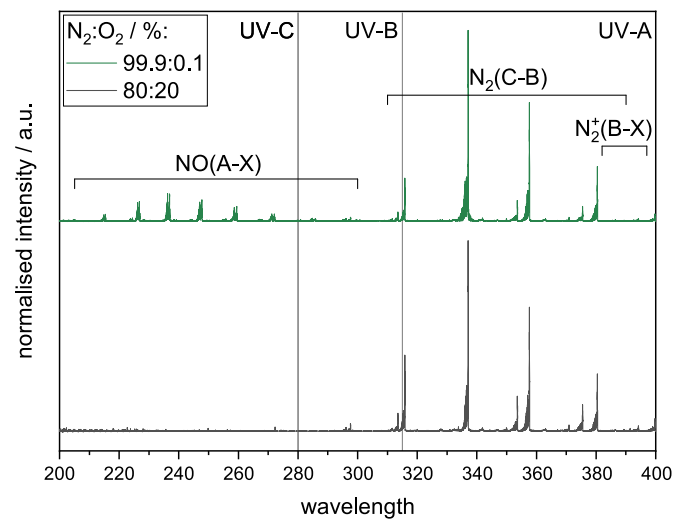


Figure 9. Example emission spectra of the DBD ignited in N₂:O₂ gas mixtures of 99.9%:≤0.1% and 80%:20% with a total gas flow of 2 slm, a HV repetition frequency of 300 Hz and an amplitude of 24 kV_{pp}. The range of the ultraviolet emission between 200 nm and 400 nm is presented.

80%:20% at 300 Hz and 24 kV_{pp}. The wavelength ranges corresponding to UV-A, -B and -C are marked. Under both conditions the second positive (N₂(C-B)) system and the first negative (N₂⁺(B-X)) system of nitrogen are observed in the UV-A range. This emission dominates the UV spectrum under most conditions studied.

4. Discussion

The discussion of the results will be divided into two parts: first, the time and power variation experiments in

Table 1. Influence of the power density on the inactivation of *B. subtilis* spores in ambient air.

V_{pp} (kV)	f (Hz)	power density (W cm ⁻¹)	CFU		ratio to lowest power	inversed ratio to lowest power	
			1 min	2 min	power density	CFU _{1 min}	CFU _{2 min}
18	300	0.05	$2.6 \cdot 10^6$	$5.9 \cdot 10^5$	—	—	—
24	300	0.2	$6.2 \cdot 10^5$	$1.3 \cdot 10^5$	4	4.1	4.5
18	1000	0.25	$7.7 \cdot 10^5$	$4.9 \cdot 10^5$	5	3.3	1.2
24	1000	0.7	$1.3 \cdot 10^5$	$1.2 \cdot 10^4$	14	20	49

ambient air will be discussed which serve as a proof-of-concept to demonstrate the possibility of inactivating spores of *B. subtilis* with an atmospheric-pressure DBD. Afterwards, the results of the experiments in defined atmospheres at intermediate power ($f = 300$ Hz, $V_{pp} = 24$ kV_{pp}) will be examined regarding different inactivation mechanisms.

Time and power variation in ambient air

The results of the time and power variation (figure 4) measurements demonstrate that *B. subtilis* spores can be inactivated by the DBD used in this study under ambient conditions. The time variation reveals a fast inactivation in the first three minutes and strong decrease of the inactivation rate for longer treatment times. In low-pressure plasmas, this effect is normally observed in the case of stacked spores where the lower spores are protected from the plasma components by the upper ones [28]. However, the sample preparation analysis shows that the treated spores are not stacked but are assembled as monolayers on the glass slides. Therefore, this effect must be a result of the plasma itself and is most-likely connected to the spatial distribution of the flux of plasma components on the sample. In the case of photons, the emission profile on the sample carrier (figure 7) shows a significant drop in the photon flux at distances above 4 mm from the center if a homogeneous emission in the plasma volume is assumed. Taking the area of the sample carrier into account, approximately 50% of the spores are located in a region where the photon flux is strongly decreasing. The same effect holds true for radical species. Previous measurements reveal that the ozone density varies approximately 3.5-fold from the center to the edge of the plasma. Regarding the density of atomic oxygen, a 6-fold reduction has been observed [31]. The implication is that the spores present in the centre of the plasma region where UV fluxes and reactive species densities are high are inactivated quickly and account for the fast decrease in CFU count at short treatment times. The slow decrease at longer treatment times can then be related to inactivation of spores in regions of lower UV irradiance and reactive species concentration at the edges of the active plasma region. This has to be kept in mind during the interpretation and discussion of the results. Since the plasma filaments are relatively homogeneously distributed, the UV fluxes as well as the radical concentrations take on a diffuse profile on the long time scales used in this study. This can also be observed in the previous profile measurements of the O and O₃ densities [31] as well as in the phase-resolved electron density distributions of the discharge published in [22].

Increasing the power by using higher peak voltages and/or frequencies results in faster inactivation. Table 1 lists the power densities and surviving CFU after 1 minute and 2 minutes treatment. In general, the inactivation rate scales quite well with power density taking into account the variation of the biological results. This suggests that increasing radical and/or photon fluxes leads to a faster inactivation, but has to be confirmed by future measurements with varying power.

Controlled dry atmosphere

Although experiments in ambient air show a reduction of *B. subtilis* spores by several orders of magnitude in a few minutes depending on the power density, the mechanisms leading to the inactivation cannot be easily analysed due to changing conditions from day to day, especially in the case of humidity. Furthermore, the role of the different photon or radical species cannot be differentiated as the gas mixture is fixed and controlled changes in the plasma chemistry are not possible. By performing inactivation experiments inside a sealed chamber the gas mixture as well as the humidity can be controlled, leading to a controlled change in plasma-produced components. In the absence of humidity in the gas phase, a decrease in the O₂ content from $\approx 99\%$ to 20% (increase in N₂ content) leads to a reduction in the ozone concentration and an increase in total UV emission. When the O₂ content is less than 0.1% the ozone concentration drops below the detection limit (3×10^{13} cm⁻³) and the total UV emission increases strongly, including a substantial increase in UV-C emission from nitric oxide (see figures 6, 8 and 9). Considering first the range of O₂ content between 20% and 99% no clear correlation between the inactivation of *B. subtilis* spores and the density of ozone can be observed. In this range, a small reduction of CFU count with time is observed that is rather independent of the ozone density. This is in strong contrast to [11] where full inactivation of different spores with a base contamination of 1×10^5 to 1×10^6 is achieved after 5 min to 10 min treatment time using an atmospheric surface microdischarge plasma source. That system was used in a closed environment with ambient air and generated an ozone concentration of 9.3 ppm which is approx. 4.7 times greater than that measured in the DBD used in this work when ignited in dry synthetic air. As both systems show similar ozone densities but different inactivation results using spores of *B. subtilis*, this effect is most-likely attributed to the relative humidity in the system. Possible inactivation mechanisms will be discussed in the respective section.

For a gas mixture of 99.9%: $\leq 0.1\%$ N₂:O₂, UV-C emission is present, without ozone, and a decrease in CFU of two orders

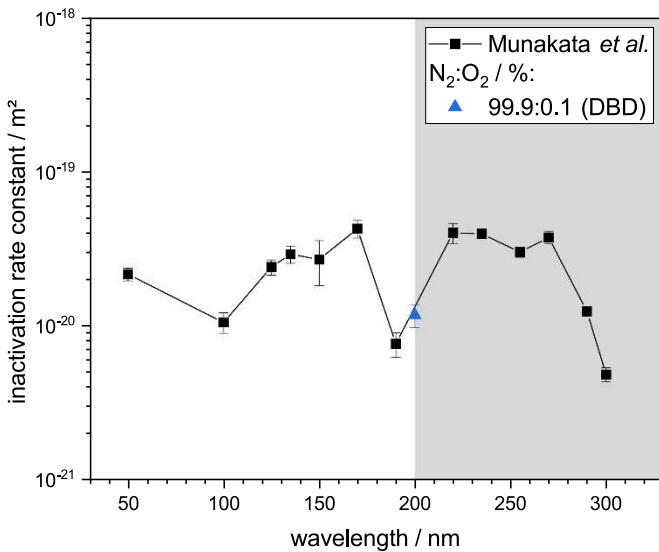


Figure 10. Inactivation rate constant of Munakata *et al* in comparison to the inactivation rate constant calculated for a treatment time of 5 min in nitrogen atmosphere. The grey area indicates the wavelength region integrated over for the calculation of the inactivation rate constant of the DBD marked as blue triangle. This is done because the DBD emits in the whole wavelength region. [37] John Wiley & Sons. © The American Society of Photobiology.

of magnitude in 5 minutes is observed. This is substantially faster than for the higher O₂ content cases where ozone is present in higher concentrations, which provides further indication that ozone is not the main driver of inactivation. In this case, the photon fluxes in the UV-C range are comparable to low pressure air plasmas that show fast deactivation. The results indicate that neither UV-A nor UV-B emission play a significant role in the inactivation of *B. subtilis* spores in this study. This finding is in accordance with inactivation experiments of Munakata *et al* applying monochromatic synchrotron radiation to *B. subtilis* spores [37]. Munakata *et al* defined an inactivation rate constant, *k*, which correlates the photon flux at a specific wavelength to the spore inactivation. By applying the same formula to a broader wavelength band (e.g. UV-C), the applicability of the *k*-factor of Munakata *et al* to the plasma experiments can be compared. The rate constant is defined as

$$k = -\ln\left(\frac{N}{N_0}\right) \frac{1}{\Gamma_{\text{photons}}}, \quad (12)$$

with *N* as the number of CFU after plasma treatment, *N*₀ indicating the initial spore load and Γ_{photons} representing the photon dose per m². Since only the spectrum of the gas mixture of 99.9%:≤0.1% N₂:O₂ is distributed throughout the UV-C range as depicted in figure 9, only this gas mixture is suitable for calculating the inactivation rate constant. The inactivation rate constant of the gas mixture 99.9%:≤0.1% N₂:O₂ and those calculated by Munakata *et al* are presented in figure 10. It can be seen that the calculated inactivation rate constant of this study correlates well with the data of Munakata *et al*. The calculated inactivation

rate constant is an integral value since all values in the UV region above 200 nm were taken into account in contrast to the data of Munakata *et al* who treated the biological samples at a specific wavelength. However, the data correlates well indicating that the inactivation efficiency of the broadband plasma emission in 99.9%:≤0.1% N₂:O₂ is comparable to the inactivation efficiency of monochromatic light. This allows the assumption that synergistic effects do not lead to the inactivation of spores in this specific gas mixture and UV-C emission is the dominant inactivation mechanism under these conditions.

For treatment times between 5 and 10 minutes the CFU count was not found to decrease further. This effect can be attributed to the inhomogeneous photon flux on the sample carrier mentioned above (see figure 7). However, the flux profile is only valid for a homogeneous emission below the whole area of the driven electrode. Since the UV-C emission is emitted by nitric oxide it will exhibit a density profile, likely similar to that of ozone, with a maximum at the center and a decrease to the edges of the electrode [31]. This would further increase the UV flux gradient from the center to the side of the sample carrier and would prolong the time required to inactivate spores located further from the center of the sample holder. Thus, a potential explanation for the inactivation kinetics observed in a gas mixture of N₂:O₂ 99.9%:0.1% is that spores in the center receive much higher fluxes of UV-C emission and NO radicals than in the outer parts and are inactivated on significantly shorter time scales.

To verify the assumption that the inactivation of *B. subtilis* spores depends on the flux profiles of the UV radiation and radicals underneath the driven electrode, spores sprayed on glass substrates were transferred via stamping onto LB agar plates after plasma treatment. Afterwards, the plates were incubated overnight at 24 °C and for 6 h at 37 °C to visualize spore revival and outgrowth in dependence of the treated sample carrier geometry. In figure 11 the results are depicted. It can be seen that colonies grow stochastically distributed within the whole area of the stamped control. After 2 min and 10 min of plasma treatment a ring-structure can clearly be seen which correlated with the treatment time. These results indicate that the inhomogeneous emission below the whole area of the driven electrode due to different flux profiles of plasma-generated species has an impact on the inactivation efficiency of the experimental setup.

Controlled humidity

To analyze the effect of humidity on the inactivation of *B. subtilis* spores the humidity content in synthetic air (N₂:O₂ 80%:20%) is controlled and the samples are treated for 1 min. By adding humidity to the gas phase the inactivation can be increased from approx. 0.5 orders of magnitude with 0% relative humidity to 2.5 orders of magnitude at 80% relative humidity. At the same time, the ozone density decreases by a factor of 4, no UV-C emission is present, and the emission in the UV-B and UV-A does not correlate with spore inactivation.

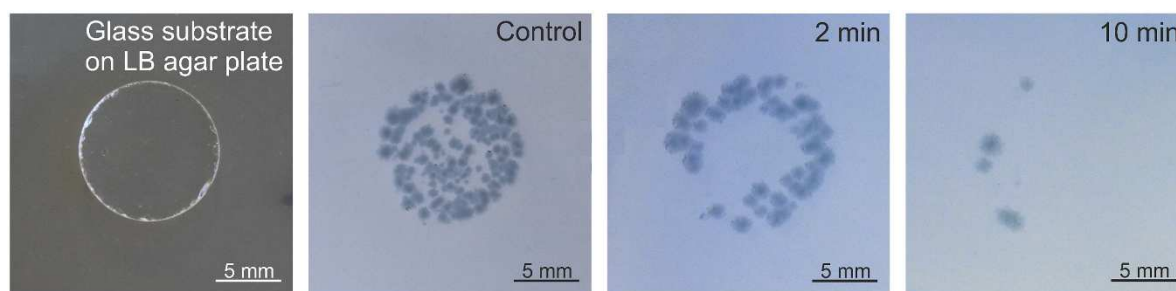


Figure 11. Image of the glass substrate on which the spores were sprayed and plasma treated in comparison to images of the growing spore colonies after no plasma treatment and plasma treatment for a duration of 2 min and 10 min. The experiments were carried out using the DBD set to 300 Hz and 24 kV_{pp}. The sprayed glass substrate was stamped onto LB agar plates. After 2 min of plasma treatment all spores in the centre of the discharge are inactivated. The area of inactivated spores in the centre of the discharge increases as a function of increasing treatment time. The colours of the images of the spores are inverted for better visibility.

Inactivation mechanisms

The results demonstrate that neither UV-B/UV-A emission nor ozone play a significant role individually in the inactivation of *B. subtilis* spores in this study. In contrast, UV-C emission (and possibly the flux of nitric oxide which emits the UV-C radiation) is effectively inactivating spores if enough photons reach the sample. This is in agreement with experiments in the low-pressure regime [27] and also known from the literature using UV-C lamps [19, 21, 29]. The strong inactivation effect due to humidity suggests a crucial influence of water-related products, such as OH, H₂O₂, or gas-phase acids such as HNO₂, HNO₃, or HO₂NO₂, which are expected to be produced in humid air plasmas [38]. Furthermore, ozone seems to be of minor importance as the inactivation of *B. subtilis* spores is uncorrelated to the ozone density. The importance of humidity has also been demonstrated by Ishizaki *et al* [39] by inactivating different *Bacillus* spores using ozone in the gas phase (250–1500 ppm) in controlled relative humidity (50%–90%). The inactivation was drastically reduced with decreasing water content and even stopped for one strain below 54%. A correlation between relative humidity (70%–95%) and inactivation efficiency of *B. subtilis* spores in ozone containing atmosphere (500–5000 ppm) was also observed by Aydogan *et al* [40]. In both studies the time needed for 1-log reduction varied between a few minutes to several hours. Furthermore, this is a possible explanation why inactivation of spores seems to be much faster using atmospheric pressure plasmas in humid air (e.g. [41]) because of the faster generation of water related species like H₂O₂.

This assumption is also supported by known inactivation mechanisms of *B. subtilis* spores from the literature: while the spore coat layers are of major importance in resisting oxidizing agents, such as ozone or peroxyxynitrite, they are only of minor importance regarding the resistance of the spore to hydrogen peroxide [19, 42, 43]. For most oxidizing agents the layers seem to act as a 'reactive armor' which detoxifies the chemicals at the outer layers of the spore coat and prevent damaging of the inner membrane, for example [42, 44]. Damaging the inner membrane may cause it to rupture during germination and result in spore death. However, the precise mechanism of the process is not known [42]. Therefore, the strong inactivation in the presence of water in the gas phase compared

to ozone might be connected to the different reactions of the molecules with the *B. subtilis* spore coat layers preventing the ozone from reaching the inner membrane while hydrogen peroxide, for example, leads to a significant damage. In addition, a few chemicals, such as formaldehyde or nitrous acid (HNO₂), are known to cause spore death by inducing DNA damage [19, 42, 45] and might play a role in the inactivation of spores if they are generated during the plasma-spore interaction. Although the damage can be observed, it is not clear how the chemicals penetrate the spore core, but a connection to the permeability of the inner membrane is assumed [42]. However, this is not the case for hydrogen peroxide as small, acid-soluble proteins (SASPs) protect the DNA [42]. Furthermore, the efficiency of water-related products might be directly connected to UV emission (UV-B, UV-A) or generated species, such as ozone, which do not have a significant effect on their own but might be necessary in the reaction pathway for spore inactivation.

5. Conclusion

Inactivation experiments are performed using *B. subtilis* spores and a non-thermal atmospheric pressure discharge, namely a dielectric barrier discharge, as well as spectroscopic measurements to determine the ozone density and the UV irradiance. The experiments are carried out in ambient air, as well as in a vacuum vessel, in order to control the atmospheric conditions, the relative N₂:O₂ mixture and humidity content. This approach offers the possibility to execute inactivation experiments with the focus on the differentiation of possible inactivation mechanisms. It can be concluded that neither UV-A and UV-B irradiance nor ozone alone contribute significantly to the inactivation of *B. subtilis* spores. Comparable with experimental results in the low-pressure regime the UV-C irradiance seems to play a role in spore inactivation under specific conditions. This conclusion is drawn due to the results obtained from the spectroscopic measurements regarding the UV irradiance as well as the ozone density. The strongest inactivation effect is evoked by humidified synthetic air, with spore inactivation directly correlating with humidity content. No positive correlation between UV irradiance or ozone concentration and spore inactivation is observed for

the humidity variation. This implies that other reactive species formed from water molecules, such as OH, H₂O₂, HNO₂, HNO₃, or HO₂NO₂, play an important role in spore inactivation. As such, consideration should be given as to how to properly control humidity content in applications in order to ensure reproducible outcomes for sterilisation processes.

In addition, the kinetics of spore inactivation demonstrate two timescales with high inactivation rates at short times, and low inactivation rates at longer times. This has been observed in previous experiments as a result of spore stacking. However, the spore spraying approach used for deposition of spores on surfaces in this work avoids this issue. In this case, the two timescale kinetics appear to be related to the spatial variation of UV irradiance and reactive species concentrations to which the sample is exposed. This leads to regions of high UV and reactive species fluxes corresponding to the fast inactivation at short times, and low UV and reactive species fluxes corresponding to slow inactivation at long times. Such effects will be important to consider in applications where reproducible inactivation is required. In particular, in applications where plasma sources are moved across surfaces systems must be designed to allow for high fluxes of UV and reactive species at all locations to be treated.

Acknowledgments

This work was funded by the German Research Foundation (DFG) with the Collaborative Research Center CRC1316 ‘Transient atmospheric plasmas: from plasmas to liquids to solids’ (projects A5 and A7) and in the frame of project ‘PlasNOW’ (430219886). R M was supported by a DLR grant DLR-FuE-project ISS LIFE (Programm RF-FuW, Teilprogramm 475) and from the German Research Foundation DFG (MO 2023/3-1).

The authors acknowledge Professor Enrique Iglesias and Dr Tilman Möller for their help regarding the calculation of the presented geometrical factor as well as Dr Jan-Wilm Lackmann for the suggestion of the LB agar plate experiments and Lars Schücke for vivid discussions.

ORCID iDs

Friederike Kogelheide  <https://orcid.org/0000-0001-9856-4338>

Felix Fuchs  <https://orcid.org/0000-0001-5669-5655>

Andrew R. Gibson  <https://orcid.org/0000-0002-1082-4359>

Katharina Stapelmann  <https://orcid.org/0000-0002-2116-2661>

Marcel Fiebrandt  <https://orcid.org/0000-0002-9877-3778>

References

- [1] Tipnis N P and Burgess D J 2018 Sterilization of implantable polymer-based medical devices: a review *Int. J. Pharm.* **544** 455–60
- [2] Kelly-Wintenberg K, Montie T, Brickman C, Roth J R, Carr A, Sorge K, Wadsworth L C and Tsai P P Y 1998 Room temperature sterilization of surfaces and fabrics with a one atmosphere uniform glow discharge plasma *J. Ind. Microbiol. Biot.* **20** 69–74
- [3] Klämpfl T G, Isbary G, Shimizu T, Li Y F, Zimmermann J L, Stolz W, Schlegel J, Morfill G E and Schmidt H U 2012 Cold atmospheric air plasma sterilization against spores and other microorganisms of clinical interest *Appl Environ Microbiol.* **78** 5077–82
- [4] Isbary G et al 2010 A first prospective randomized controlled trial to decrease bacterial load using cold atmospheric argon plasma on chronic wounds in patients *Br. J. Dermatol.* **163** 78–82
- [5] Brehmer F, Haenssle H, Daeschlein G, Ahmed R, Pfeiffer S and Görlitz A et al 2015 Alleviation of chronic venous leg ulcers with a hand-held dielectric barrier discharge plasma generator (PlasmaDerm® VU-2010): results of a monocentric, two-armed, open, prospective, randomized and controlled trial (NCT 01415622) *J. Eur. Acad. Dermatol. Venereol.* **29** 148–55
- [6] Ulrich C et al 2015 Clinical use of cold atmospheric pressure argon plasma in chronic leg ulcers: a pilot study *J. Wound Care* **24** 196–203
- [7] Flynn P B, Higginbotham S, Nida H A, Gorman S P, Graham W G and Gilmore B F 2015 Bactericidal efficacy of atmospheric pressure non-thermal plasma (APNTP) against the ESKAPE pathogens *Int. J. Antimicrob. Agents* **46** 101–7
- [8] Connor M, Flynn P B, Fairley D J, Marks N, Manesiotis P, Graham W G, Gilmore B F and McGrath J W 2017 Evolutionary clade affects resistance of *Clostridium difficile* spores to cold atmospheric plasma *Sci. Rep.* **7** 41814
- [9] Krewing M, Jarzina F, Dirks T, Schubert B, Benedikt J, Lackmann J W and Bandow J E 2019 Plasma-sensitive *Escherichia coli* mutants reveal plasma resistance mechanisms *J. R. Soc. Interface* **16** 20180846
- [10] Reineke K, Langer K, Hertwig C, Ehlbeck J and Schlüter O 2015 The impact of different process gas compositions on the inactivation effect of an atmospheric pressure plasma jet on *Bacillus* spores *Innov. Food. Sci. Emerg.* **30** 112–18
- [11] Klämpfl T G et al 2014 Decontamination of nosocomial bacteria including *clostridium difficile* spores on dry inanimate surface by cold atmospheric plasma *Plasma Process Polym.* **11** 974–84
- [12] Heuer K et al 2015 The topical use of non-thermal dielectric barrier discharge (DBD): nitric oxide related effects on human skin *Nitric Oxide* **44** 52–60
- [13] Suschek C V and Opländer C 2016 The application of cold atmospheric plasma in medicine: the potential role of nitric oxide in plasma-induced effects *Clin. Plasma Med.* **4** 1–8
- [14] Emmert S et al 2013 Atmospheric pressure plasma in dermatology: ulcer treatment and much more *Clin. Plasma Med.* **1** 24–9
- [15] Assadian O, Ousey K J, Daeschlein G, Kramer A, Parker C, Tanner J and Leaper D J 2019 Effects and safety of atmospheric low-temperature plasma on bacterial reduction in chronic wounds and wound size reduction: a systematic review and meta-analysis *Int. Wound J.* **16** 103–11
- [16] Driks A 2002 Overview: development in bacteria: spore formation in *Bacillus subtilis* *Cell. Mol. Life Sci.* **59** 389–91
- [17] Schroeder J W and Simmons L A 2013 Complete genome sequence of *Bacillus subtilis* strain PY79 *Genome Announc* **1** e01085–13
- [18] Driks A and Eichenberger P 2016 The spore coat *The Bacterial Spore: From Molecules to Systems* (New York: Wiley) pg 179–200
- [19] Setlow P 2007 I will survive: DNA protection in bacterial spores *Trends Microbiol.* **15** 172–80

- [20] McKenney P T, Driks A and Eichenberger P 2013 The *Bacillus subtilis* endospore: assembly and functions of the multilayered coat *Nat. Rev. Microbiol.* **11** 33
- [21] Setlow P and Li L 2015 Photochemistry and photobiology of the spore photoproduct: a 50-year journey *Photochem. Photobiol.* **91** 1263–90
- [22] Kogelheide F, Offerhaus B, Bibinov N, Krajinski P, Schütcke L, Schulze J, Stapelmann K and Awakowicz P 2019 Characterisation of volume and surface dielectric barrier discharges in N₂/O₂ mixtures using optical emission spectroscopy *Plasma Process Polym.* **2019** e1900126
- [23] Schaeffer P, Millet J and Aubert J P 1965 Catabolic repression of bacterial sporulation *Proc. Natl Acad. Sci. Am.* **45** 704–11
- [24] Nicholson W L and Setlow P 1990 Sporulation, germination and outgrowth *Molecular Biological Methods for Bacillus* ed Harwood C R and Cutting S M (Sussex: Wiley) pp 391–450
- [25] Nagler K, Setlow P, Li Y Q and Moeller R 2014 High salinity alters the germination behavior of *Bacillus subtilis* spores with nutrient and nonnutrient germinants *Appl. Environ. Microbiol.* **80** 1314–21
- [26] Rose R, Setlow B, Monroe A, Mallozzi M, Driks A and Setlow P 2007 Comparison of the properties of *Bacillus subtilis* spores made in liquid or on agar plates *J. Appl. Microbiol.* **103** 691–9
- [27] Fiebrandt M, Hillebrand B, Lackmann J W, Raguse M, Moeller R, Awakowicz P and Stapelmann K et al 2018 Inactivation of *B. subtilis* spores by low pressure plasma—influence of optical filters and photon/particle fluxes on the inactivation efficiency *J. Phys. D: Appl. Phys.* **51** 045401
- [28] Raguse M et al 2016 Improvement of biological indicators by uniformly distributing *Bacillus subtilis* spores in monolayers to evaluate enhanced spore decontamination technologies *Appl. Environ. Microbiol.* **82** 2031–8
- [29] Moeller R, Setlow P, Reitz G and Nicholson W L 2009 Roles of small, acid-soluble proteins and core water content in survival of *Bacillus subtilis* spores exposed to environmental solar UV radiation *Appl. Environ. Microbiol.* **75** 5202–8
- [30] Offerhaus B, Lackmann J W, Kogelheide F, Bracht V, Smith R, Bibinov N, Stapelmann K and Awakowicz P 2017 Spatially resolved measurements of the physical plasma parameters and the chemical modifications in a twin surface dielectric barrier discharge for gas flow purification *Plasma Process Polym.* **14** 1600255
- [31] Baldus S, Schröder D, Bibinov N, Schulz-von der Gathen V and Awakowicz P 2015 Atomic oxygen dynamics in an air dielectric barrier discharge: a combined diagnostic and modeling approach *J. Phys. D: Appl. Phys.* **48** 275203
- [32] Herzig H, Toft A R and Fleetwood C M 1993 Long-duration orbital effects on optical coating materials *Appl. Opt.* **32** 1798–804
- [33] Hunter W 1998 11. Reflectance spectra of single materials *Experimental Methods in the Physical Sciences* (Amsterdam: Elsevier) vol 31 pp 205–26
- [34] Griggs M 1968 Absorption coefficients of ozone in the ultraviolet and visible region *J. Chem. Phys.* **49** 857–69
- [35] Barnes J and Mauersberger K 1987 Temperature dependence of the ozone absorption cross section at the 253.7-nm mercury line *J. Geophys. Res.* **92** 14861–4
- [36] Danielak J, Domin U, Kepa R, Rytel M and Zachwieja M 1997 Reinvestigation of the emission gamma band system ($A^2\Sigma^+-X^2\Pi$) of the NO molecule *J. Mol. Spectrosc.* **181** 394–402
- [37] Munakata N, Saito M and Hieda K 1991 Inactivation action spectra of *Bacillus subtilis* spores in extended ultraviolet wavelengths (50–300nm) obtained with synchrotron radiation *Photochem. Photobiol.* **54** 761–8
- [38] Lietz A M and Kushner M J 2016 Air plasma treatment of liquid covered tissue: long timescale chemistry *J. Phys. D: Appl. Phys.* **49** 425204
- [39] Ishizaki K, Shinriki N and Matsuyama H 1986 Inactivation of *Bacillus spores* by gaseous ozone *Plasma Process Polym.* **60** 67–72
- [40] Aydogan A and Gurol M D 2006 Application of gaseous ozone for inactivation of *Bacillus subtilis* spores *J. Air Waste Manage.* **56** 179–85
- [41] Müller M, Shimizu T, Binder S, Rettberg P, Zimmermann J L, Morfill G E and Thomas H 2018 Plasma afterglow circulation apparatus for decontamination of spacecraft equipment *AIP Adv.* **8** 105013
- [42] Setlow P 2006 Spores of *Bacillus subtilis*: their resistance to and killing by radiation, heat and chemicals *J. Appl. Microbiol.* **101** 514–25
- [43] Young S and Setlow P 2004 Mechanisms of *Bacillus subtilis* spore resistance to and killing by aqueous ozone *J. Appl. Microbiol.* **96** 1133–42
- [44] Setlow P 2016 Spore resistance properties *The Bacterial Spore: From Molecules to Systems* (Chicago, IL: American Society of Microbiology) pp 201–15
- [45] Leyva-Illades J F, Setlow B, Sarker M R and Setlow P 2007 Effect of a small, acid-soluble spore protein from *Clostridium perfringens* on the resistance properties of *Bacillus subtilis* spores *J. Bacteriol.* **189** 7927–31